The skeletal muscle circadian clock regulates sarcomere length homeostasis through titin splicing

Lance A. Riley[1,5,#], Xiping Zhang[1,5], Joseph M. Mijares[1,5], David W. Hammers[2,5], Hailey R. Olafson[4], Ping Du[1], Collin M. Douglas[1,5], Siegfried Labeit[3], Eric T. Wang[4,5], and Karyn A. Esser[1,5,*]

[1] Department of Physiology and Functional Genomics, University of Florida, Gainesville, FL 32610
[2] Department of Pharmacology and Therapeutics, University of Florida, Gainesville, FL 32610
[3] Medical Faculty Mannheim, University of Heidelberg, 68161 Mannheim, Germany
[4] Department of Molecular Genetics of Microbiology, Center for Neurogenetics, University of Florida, Gainesville, FL 32610
[5] Myology Institute, University of Florida, Gainesville, FL 32610
[#] Present Address: Department of Biomedical Engineering, Vanderbilt University, Nashville, TN 37232
*Karyn A. Esser

Email: kaesser@ufl.edu

Author Contributions: L.A.R. and K.A.E. designed research; L.A.R., J.M.M., D.W.H., X.Z., and C.M.D. performed research; S.L. and E.T.W. contributed tools/reagents; L.A.R., J.M.M., X.Z., H.R.O., and K.A.E. analyzed data; and L.A.R and K.A.E. wrote the manuscript with contributions from all other authors.

Competing Interest Statement: The authors declare no competing interests.

Classification: BIOLOGICAL SCIENCES - Physiology

Keywords: Titin, Skeletal muscle, Circadian rhythms, BMAL1, Sarcomere

This PDF file includes:

Main Text
Figures 1 to 6

Abstract

Circadian rhythms in skeletal muscle are maintained by a transcriptional-translational feedback loop known as the molecular clock. While previous research suggested a role for the molecular clock in regulating skeletal muscle structure and function, no mechanisms have connected the molecular clock to sarcomeric proteins. Utilizing inducible, skeletal muscle specific, *Bmal1* knockout (iMS*Bmal1*$^{-/-}$) mice, we show that deletion of the skeletal muscle molecular clock alters titin isoform and skeletal muscle sarcomere length. We then use U7 snRNPs in myotubes to directly alter titin splicing *in vitro*. Truncating titin's proximal Ig domain results in altered sarcomere length. Finally, we identify a mechanism whereby the skeletal muscle molecular clock regulates titin isoform expression through RBM20, a potent splicing regulator of the titin transcript. Our findings demonstrate the importance of the skeletal muscle molecular clock in maintaining sarcomere length homogeneity through its regulation of RBM20 expression. Because circadian rhythm disruption is a feature of many diseases, our results highlight a pathway that could be targeted to maintain skeletal muscle structure and function in a range of pathologies.

Significance Statement

Circadian rhythms regulate many aspects of skeletal muscle physiology; however, the exact mechanisms connecting the molecular underpinnings of these rhythms to skeletal muscle structure and function are poorly understood. Here we describe how the skeletal muscle molecular clock regulates titin, the protein ruler regulating sarcomere length and muscle strength. Since circadian rhythms and skeletal muscle weakness underly a number of diseases, these results highlight a potential target for future therapeutic strategies.

Introduction

Circadian rhythms are patterns in biological processes that oscillate approximately every 24-hours (1). Underlying circadian rhythms is a transcriptional-translational, negative feedback loop referred to as the molecular clock. The molecular clock exists in virtually every cell in the body and functions to support homeostasis through regulating a daily pattern of gene expression (2, 3).

BMAL1 is a PAS/basic helix-loop-helix (bHLH) transcription factor that acts as the only non-redundant component of the core clock mechanism (4, 5). Beyond its role in cellular time keeping, BMAL1 and its partner, CLOCK, have been described as transcriptional regulators of genes important for cell-type specific functions (1, 6, 7). The most well studied aspects of these functions, particularly in context of skeletal muscle, is the timing of both carbohydrate and lipid metabolism (8). Our lab has provided evidence suggesting a more expansive role for the skeletal muscle molecular clock: Maintenance of skeletal muscle structure and function (9–11).

The first evidence for this potential role was microarray analyses showing expression of the myogenic regulatory factor *MyoD1* and expression of genes encoding contractile proteins are circadian in the hindlimb muscles of C57BL/6J mice (9). The molecular clock's proposed role in maintaining muscle function was supported with whole muscle and single fiber mechanics data from the *Bmal1* knockout mice (10). Additionally, electron microscopy studies demonstrated sarcomere irregularities consistent with the diminished force output findings. However, these experiments were performed in systemic *Bmal1* KO mice that exhibit significant behavioral abnormalities, thus, distinguishing the role of skeletal muscle molecular clock from activity patterns requires further study using more refined approaches and animal models.

This study utilized inducible, skeletal muscle specific *Bmal1* (iMS*Bmal1*$^{-/-}$) mice to further examine the role of the skeletal muscle molecular clock in regulating sarcomere structure. Importantly, these mice display muscle weakness defined by *ex vivo* measures of maximum isometric tetanic force (i.e., specific force) (11). We show that disruption of circadian rhythms specifically in adult skeletal muscle disrupts sarcomere length homogeneity through changes in splicing of titin's spring region. Mechanistically, the skeletal muscle molecular clock targets RBM20, an RNA-binding protein known to regulate titin splicing, and that overexpressing RBM20 in iMS*Bmal1*-/- skeletal muscle is sufficient to restore titin isoform expression. Our findings establish the role of the skeletal muscle molecular clock in regulating sarcomere structure and provide a mechanism by which circadian dysregulation might alter skeletal muscle function.

Results

iMSBmal1$^{-/-}$ muscle displays irregular sarcomere lengths and a titin isoform switch

Since the global knockout of *Bmal1* leads to sarcomere abnormalities in skeletal muscle, we first tested if these observations are specifically due to loss of skeletal muscle *Bmal1* or due to loss of behavioral rhythms and/or other systemic interactions (10). We utilized the iMS*Bmal1*$^{-/-}$ mouse model in which *Bmal1* is specifically knocked out only in adult skeletal muscle following (11, 12). These mice retain normal activity rhythms and we previously published that specific force is significantly reduced similar to the global *Bmal1* KO muscle. To determine if iMS*Bmal1*$^{-/-}$ skeletal muscle presents with abnormal sarcomere morphology to accompany the weakness, we longitudinally cryosectioned TA muscles from iMS*Bmal1*$^{+/+}$ and iMS*Bmal1*$^{-/-}$ mice at 5-weeks post-recombination and visualized sarcomeres via α-actinin immunostaining (Figure 1A). Using this approach, mean sarcomere length did not significantly change following skeletal muscle specific loss of *Bmal1* ($P = 0.86$; Figure 1B). However, sarcomere length homogeneity is a feature of healthy striated muscle and we noted that sarcomere length was significantly more variable in iMS*Bmal1*$^{-/-}$ muscle compared to iMS*Bmal1*$^{+/+}$ muscle ($F = 22.12$, $P < 0.05$; Figure 1B).

Titin splicing is disrupted following Bmal1 knockout in adult skeletal muscle

Since titin has been implicated in regulating sarcomere length and plays a prominent role in striated muscle force generation, we tested if titin protein changes following *Bmal1* knockout in

skeletal muscle. Using SDS-vertical agarose gel electrophoresis (SDS-VAGE) to analyze iMS*Bmal1*$^{-/-}$ TA muscle, we found a shift in titin isoform composition ($P < 0.01$; Figure 2A and 2B) with no change in total titin expression. The shift in titin isoforms changes the predominant form from a short isoform to a mixture of both short and long titin proteins. This increase in the mix of titin lengths is consistent with the observed sarcomere length heterogeneity.

Titin mRNA undergoes large amounts of alternative splicing to generate its many isoforms (13). To gain insight into the titin isoform switch following loss of *Bmal1* in adult skeletal muscle, we performed RNA sequencing to test if loss of *Bmal1* leads to a change in titin spliceform (14–16). iMS*Bmal1*$^{-/-}$ TA muscle showed increased inclusion of exons 51-89 of the titin transcript compared to iMS*Bmal1*$^{+/+}$ control samples (Figure 2C). These exons code for a portion of titin's proximal Ig segment, one of titin's extensible segments within its spring region. Though the ∆PSI across this splicing event was stable, the variability in PSI across this event made statistical analysis difficult. To remedy this, we split this large splicing event into three smaller splicing events based on the similarity of PSI values within each sample (Figure 2C). In each of these smaller events, inclusion of exons was significantly greater in iMS*Bmal1*$^{-/-}$ muscle compared to iMS*Bmal1*$^{+/+}$ muscle (Figure 2D; $P < 0.05$). Thus, *Bmal1* knockout in skeletal muscle altered splicing of titin's II band localized spring region and may account for the sarcomere length irregularities.

Titin isoform shift accounts for sarcomere length irregularity in iMSBmal1$^{-/-}$ *muscle*

After determining the region of titin mRNA that changed in iMS*Bmal1*$^{-/-}$ muscle, we asked if this splicing change could account for the increased sarcomere length variability. To test this, we performed immunohistochemistry using epitope-specific antibodies against titin's Z1Z2 and N2A domains because these regions flank the proximal Ig segment of titin. Thus, the positional difference between the two domains provides a proxy for proximal Ig domain length (Figure 3A). Representative images of iMS*Bmal1*$^{+/+}$ and iMS*Bmal1*$^{-/-}$ muscle can be seen in Figures 3B and 3C, respectively. The significant difference in sarcomere length variability persisted though the lengths themselves were longer than in our previous measurements. iMS*Bmal1*$^{+/+}$ muscle had sarcomere lengths of 2.115 ± 0.014 µm while iMS*Bmal1*$^{-/-}$ muscle had sarcomere lengths of 2.278 ± 0.024 µm ($F = 3.619$, $P < 0.001$; Figure 3D). Once we determined that sarcomere length variability was maintained, we asked if proximal Ig domain length was significantly altered following *Bmal1* knockout in adult skeletal muscle. iMS*Bmal1*$^{-/-}$ had significantly longer proximal Ig domain lengths (229.5 ± 1.357 nm) than the proximal Ig domain from iMS*Bmal1*$^{+/+}$ samples (182.4 ± 1.388 nm; $P < 0.0001$; Figure 3E). This difference in lengths accounts for the difference we see in sarcomere lengths in these samples. However, the variation around the mean for proximal Ig domain length was not significantly different ($F = 1.338$, $P = 0.12$). These changes confirm that the proximal Ig domain length in adult skeletal muscle is correlated with a corresponding change in sarcomere length.

Changes in titin I-band splicing are directly linked to changes in sarcomere length

While the changes to sarcomere length of iMS*Bmal1*$^{-/-}$ TA muscle seem to be directly associated with titin, other transcriptional and splicing changes occur in this mouse that potentially confound our results. Notably, we see 120 differentially expressed genes through our RNAseq analysis ($P_{adj} < 0.05$; Supplementary Table 4) and 807 differentially expressed exons across 636 genes ($P_{adj} < 0.01$; Supplemental Dataset 1). Further, PANTHER gene ontology analysis identified enriched GO categories among differentially spliced genes include sarcomere structure and dilated cardiomyopathy (Supplementary tables 5-7). These categories would be expected in conditions where titin is altered; however, we cannot rule them out as contributing to sarcomere length variability following skeletal muscle Bmal1 knockout. To directly test titin length and sarcomere length, we used U7 snRNPs to direct titin splicing from the 5' splice site of titin exon 51 to the 3' splice site of titin exon 89 in an in vitro C2C12 model. To visualize sarcomere length, we used a stable cell line in which alpha actinin is labeled with GFP (i.e. eGFP-ACTN2-C2C12). These labeled myocytes were transfected with the titin-specific U7 snRNPs and plated on micropatterned gelatin hydrogels to support maturation of the myotube culture and sarcomere formation (17, 18). At day 10 of differentiation, eGFP-ACTN2-C2C12 myotubes were fixed then stained with titin epitope-

specific antibodies similarly to the tissue samples from iMS*Bmal1*$^{-/-}$ muscle (Figure 4A). Representative images of control eGFP-ACTN2-C2C12 myotubes and *Ttn*-U7 transfected eGFP-ACTN2-C2C12 myotubes can be seen in Figures 4B and 4C, respectively. While control myotubes had an average sarcomere length of 2.756 ± 0.0495 μm, *Ttn*-U7 transfected myotubes had significantly shorter sarcomeres with an average sarcomere length of 2.387 ± 0.0347 μm (P < 0.0001, n = 100-200 sarcomeres/2 biological replicates; Figure 4D). Because ACTN2 is a key component of the Z-line, the distance between the N2A-epitope and eGFP-ACTN2 was used to calculate proximal Ig length in this experiment. Proximal Ig domain lengths were also significantly different. *Ttn*-U7 transfected myotubes had a proximal Ig length of 285.1 ± 3.131 nm compared to 448.0 ± 3.368 nm of control myotubes (P < 0.0001; Figure 4E). These results confirm that altering the length of titin's proximal Ig domain causes a change in sarcomere length in skeletal muscle myotubes.

Rbm20 is targeted by the skeletal muscle molecular clock

Having established that iMS*Bmal1*$^{-/-}$ skeletal muscle has an altered titin isoform composition resulting in sarcomere length heterogeneity, we looked to define the mechanism linking the skeletal muscle molecular clock to titin splicing. RBM20 is a well-characterized splicing factor known to target titin pre-mRNA (15, 16, 19). RBM20 is an RNA-binding protein that acts as a splicing repressor such that when present at high levels, it binds along titin pre-mRNA preventing normal intronic splicing. When bound by many RBM20 proteins, titin pre-mRNA undergoes large exon skipping events whereby the resultant, processed mRNA is shorter than if RBM20 was not present. We tested whether RBM20 levels change following loss of skeletal muscle *Bmal1*. *Rbm20* mRNA expression was reduced by 34% in iMS*Bmal1*$^{-/-}$ muscle compared to iMS*Bmal1*$^{+/+}$ muscle (Figure 5A; P < 0.05). This reduced expression was also present at the protein level where RBM20 protein content decreased 46% compared to iMS*Bmal1*$^{+/+}$ muscle (Figure 5B; P < 0.05).

Since skeletal muscle *Bmal1* knockout reduced RBM20 expression, we asked if this is due to direct regulation by the skeletal muscle molecular clock or through secondary means. We queried our publicly available MYOD1, BMAL1, and CLOCK ChIP-Seq datasets where gastrocnemius muscles were used to define the clock factor binding landscape (20–22). These data were used because our lab recently showed that MYOD1, a myogenic regulatory factor, and BMAL1::CLOCK can cooperatively transcribe genes as part of a muscle-specific clock network and can be detected in shared binding peaks in over 3000 genes (20, 22). As seen in Figure 5C, MYOD1, BMAL1, and CLOCK binding overlap within *Rbm20*'s first intron. Analysis of this region identified a putative regulatory element as defined by the third phase of the ENCODE project (23). To confirm binding of the skeletal muscle molecular clock at this site, we performed MYOD1, BMAL1, and CLOCK ChIP-PCR using primers flanking this site. We identified significant binding of MYOD1 (P < 0.001), BMAL1 (P < 0.01), and CLOCK (P < 0.001) (Figure 5D). These results are consistent with a model where the core clock factors, with MYOD1, function to directly or indirectly regulate expression of *Rbm20*.

RBM20 overexpression in iMSBmal1-/- muscle restores titin isoform expression

Since the clock components in skeletal muscle bind within a putative regulatory element in *Rbm20* and RBM20 expression decreases in iMS*Bmal1*$^{-/-}$ skeletal muscle, we rescued RBM20 expression in the iMS*Bmal1*$^{-/-}$ model using AAV expression of *Rbm20* to determine if restoring expression of this protein restores titin splicing and protein uniformity (Figure 6A). In iMS*Bmal1*$^{-/-}$ muscle injected with GFP-AAV, RBM20 protein decreased 38% compared to iMS*Bmal1*$^{+/+}$ muscle injected with GFP-AAV (P < 0.05). Injection of RBM-AAV into iMS*Bmal1*$^{-/-}$ muscle increased RBM20 protein expression by almost 2-fold above wildtype iMS*Bmal1*$^{+/+}$-GFP-AAV levels (P < 0.05; Figure 6B). We performed SDS-VAGE with these muscles to determine titin isoform distribution. Consistent with earlier work, loss of muscle Bmal1 resulted in a significant increase in the long form of titin; (P < 0.01; Figure 6C). AAV expression of RBM20 in the iMSBmal1-/- muscle was sufficient to significantly reduce the amount of the long titin isoform to levels closer to wildtype (P < 0.05;

Figure 6C). These findings demonstrate that changes in RBM20 expression downstream of the muscle clock contribute, in part, to titin isoform heterogeneity in skeletal muscle.

Discussion

In this study, we examined the skeletal muscle circadian clock's regulation of sarcomere structure. We defined a novel mechanism whereby the skeletal muscle clock regulates sarcomere length homogeneity by controlling *Rbm20*, a potent regulator of titin splicing. These findings highlight the role of the skeletal muscle clock in modulating skeletal muscle structure and function (7, 9–11, 20). The novel link between the molecular clock and RBM20 is of particular importance in this work. Our lab recently proposed a mechanism whereby MYOD1 works with BMAL1::CLOCK to cooperatively regulate skeletal muscle specific, clock-controlled genes (20). Binding of all three transcription factors within a putative regulatory region of *Rbm20* suggests that *Rbm20* is a clock-controlled gene in skeletal muscle. We additionally provide direct evidence that changes to the proximal Ig segment of titin's spring region can alter sarcomere length and yield further support for titin's role as a molecular ruler. Our findings expand upon the importance of the molecular clock in maintaining skeletal muscle health by showing that circadian rhythms are not only important for the metabolic function of this tissue but also for maintaining its structural integrity.

Defining mechanisms to preserve muscle function is important due to the emerging recognition that maintaining muscle strength in chronic disease states and aging is necessary to prolong the healthspan (24). Since skeletal muscle function is tightly linked to its structure, we investigated a mechanism that links the molecular clock to sarcomere organization in skeletal muscle. One of the findings of the current study is an increase in sarcomere length heterogeneity following skeletal muscle *Bmal1* knockout. Heterogeneous sarcomere lengths would be disadvantageous at the muscle tissue level as the likelihood that an individual sarcomere would be operating at its optimal length is reduced. While a sarcomere can generate force outside of optimal length, it is well established that the number of crossbridges between the thin and thick filaments is reduced thus lowering the maximum force produced by the muscle. Sarcomere length heterogeneity leading to suboptimal myofilament overlap is likely a contributing mechanism for the muscle weakness seen in iMS*Bmal1*-/- mice and has not been studied as a possible contributor to muscle weakness in a variety of disease states.

RBM20 is a highly conserved splicing repressor that is predominantly expressed in both cardiac and skeletal muscles. It is well studied in cardiac muscle as mutations are linked to cardiomyopathies (15), however, its role in skeletal muscle has largely remained understudied (13). We showed that RBM20 expression is decreased following *Bmal1* knockout, *Rbm20* is directly bound by BMAL1, CLOCK, and MYOD1, and rescuing RBM20 expression restores titin homogeneity. Our findings uncover the importance of the relationship between the circadian clock, RBM20, and sarcomere structure. It is also important to note that RBM20 expression is currently linked to splicing of up to 30 mRNAs in the heart. Thus, regulation of RBM20 downstream of the circadian clocks could contribute to other aspects of muscle weakness independent of titin splicing. Since circadian rhythm disruption occurs in many pathologies, our findings suggest RBM20 and titin splicing could play a broader role in diseases with concomitant weakness.

Why the molecular clock would regulate a protein as large as titin is puzzling. Estimations of titin turnover have been measured on the order of days, much longer than processes that would predictably be regulated downstream of circadian rhythms (25). However, studies in cardiomyocytes suggest that sarcomeric titin exhibits dynamic exchange within ~14 hours independent of protein turnover (26). If such a mechanism exists in skeletal muscle, this would allow the fiber to modulate titin length on a daily basis. Most recently, our lab has identified titin-cap (Tcap), a protein that anchors the titin filament at the Z-line by binding titin's Z1Z2 domain, as a clock-controlled gene (27, 28). Titin-cap's protein levels change over time of day with highest levels during the active phase (29, 30). These observations suggest a model in which titin protein could be exchanged daily, likely in sync with times at which Tcap protein is lowest. This daily

replacement would serve to provide flexibility in the muscle fibers to adjust to patterns of use and disuse.

This study uniquely links the field of circadian rhythms with well-established properties of skeletal muscle structure and function. Since maintenance of circadian rhythms and skeletal muscle strength are gaining recognition for their roles in human health, understanding these processes is needed to promote health. Our work provides important new insights for understanding fundamental mechanisms regulating muscle homeostasis and they also provide potential new targets through which diseases that modulate the circadian clock could lead to skeletal muscle weakness.

Materials and Methods

Animal Studies

The iMS*Bmal1* mouse model has been described (11, 12). The *Bmal1*^{lox} mouse was purchased from Jackson laboratories (stock number 7668) and crossed with the skeletal muscle-specific Cre-recombinase mouse (HSA-Cre) generated in-house (31). All experiments were performed in male mice housed in an AAALAC regulated facility under 12h light-12h dark cycle with ad libitum food and water availability. Breeding for iMS*Bmal1*$^{fl/fl}$ mice was performed as described in Hodge et al. (2015), and recombination was induced in 12-16 week old male mice through intraperitonial vehicle (15% ethanol in sunflower seed oil) or tamoxifen injections (2 mg day-1) for five days (12). Five weeks after injections were completed, mice were sacrificed through cervical dislocation and tissues were collected. Tissues were flash frozen in liquid nitrogen and stored at -80°C for RNA and protein analysis. All animal procedures were approved by the University of Kentucky's and University of Florida's Institutional Animal Care and Use Committees.

Immunohistochemistry

Tibialis anterior (TA) muscles were pinned at slack length on a cork block, flash frozen in OCT compound (Tissue-Tek) in liquid nitrogen cooled isopentane, and stored at -80°C. Muscles were longitudinally sectioned at 6 µm and fixed with 2% paraformaldehyde. Sections were permeabilized using 0.1% Tween 20 in PBS, blocked with BSA, and incubated overnight at 4°C with primary antibodies (Supplementary Table 1). Tissue sections were washed with PBS then incubated for 1 hour at room temperature with Alexa Fluor conjugated secondary antibodies (Thermo-Fisher) prior to mounting with ProLong Gold (Molecular Probes).

Sections with only α-actinin were imaged using Leitz DMRBE microscrope with a Leica DCF480 digital camera. Sarcomere lengths were measured using the 1D line tool within ImageJ as the distance between peak fluorescence signals. For titin-epitope specific immunohistochemistry, sections were permeabilized using 0.1% Tween 20 in PBS, blocked with 10% BSA 5% goat serum in permeabilization buffer, and incubated overnight at 4˚C for each of the primary antibodies. Secondary antibodies were added for 1 hour at room temperature between primary antibodies. Sections with titin epitope-specific antibody staining were imaged using a Leica TCS-SP8 confocal microscope equipped with Hyvolution deconvoltion software. Measurements were made using Leica LASX software.

Vertical Agarose Gel Electrophoresis

TA muscles were pulverized under liquid nitrogen using a mortar and pestle to prevent fiber type and muscle region bias. Muscle powder was dissolved in sample buffer consisting of 8M urea, 2M thiourea, 0.05M Tris base, 75mM DTT, and 3% SDS at a 60:1 volume-muscle ratio to ensure titin solubilization (32). Protein concentrations were measured using the RC-DC protein assay (Bio-Rad) and stored at -80°C until use. Samples were resolved on a vertical agarose gel consisting of 1.0% w/v Seakem Gold Agarose (Lonza), 30% glycerol, 50 mM Tris base, 0.384 M glycine, 0.1% SDS run at 5 mA/gel for 30 minutes then 7.5 mA/gel for 4 hours at 4°C (32). Titin protein was visualized using Sypro Ruby (Invitrogen) and imaged using a ChemiDoc MP System (Bio-Rad) at 450 nm. Bands were densitometrically analyzed using BioRad ImageLab software as

long T1 titin (upper), short T1 titin (lower), T2 titin (a major titin degradation product), and total titin (all bands combined).

RNA Isolation and RNA Sequencing

RNA was isolated using procedures common to our lab for next-generation RNA sequencing (11, 12, 24). Briefly, muscle powder was homogenized in TRIzol (Invitrogen) according to the manufacturer's directions then isolated using Qiagen RNeasy mini kit. RNA samples were treated with TURBO DNase (Ambion) to remove genomic DNA. RNA integrity numbers (RIN) were determined using the Agilent 2100 Bioanalyzer. RNA samples with RIN values greater than 8 were used for sequencing library preparation. 250 ng of total RNA was used to prepare barcoded RNA-seq libraries using Stranded RNA-Seq Kit with RiboErase (KAPA Biosystems). Samples were sequenced on the HiSeq 2500 (Illumina) using a 2x100 kit to a read depth >45 million reads/sample (Supplementary Table 2). Reads were checked using FastQC before mapped to mm10 with HISAT2 (33). Gene expression data were collected using HTSeq and DESeq2 analysis packages (34), and splicing analysis was performed using the protocol outlined by Schafer et. al, (2015) (14). Exon usage data is reported as percent spliced in (PSI) and change in PSI (ΔPSI; iMS*Bmal1*$^{-/-}$ - iMS*Bmal1*$^{+/+}$). Data has been deposited to GEO (GSE172067).

Cell Culture

Our generation of eGFP labeled α-actinin-2 C2C12 cells has been previously described (17). Myoblasts were maintained on plastic cell culture dishes in Dulbecco's Modified Eagle Medium (DMEM) supplemented with 10% fetal bovine serum and 1% penicillin-streptomycin in a humidified incubator kept at 37°C and 5% CO2. When cells reached 70% confluency, they were separated and plated on micropatterned gelatin hydrogels. Gelatin hydrogels and PDMS stamps used for patterning were prepared as previously described (17, 18). Once 100% confluent, cells were serum restricted with differentiation medium (DMEM, 2% horse serum, 1% penicillin-streptomycin) and left to differentiate for 10 days. Media were replenished each day.

Titin-Specific U7 snRNPs

Titin-specific, modified U7 snRNAs were generated using methods previously published to direct dystrophin splicing (35–37). The donor splice site on exon 51 and the acceptor splice site on exon 89 were targeted to induce the exon skipping event studied through RNA sequencing of iMS*Bmal1*$^{-/-}$ and iMS*Bmal1*$^{+/+}$ muscle. Sequences were generated to block these splice sites according to published standards and cloned into pAAVsc-CB6-PI-mCherry (37). Briefly, a base U7smOpt vector was generated from the wildtype U7 snRNA gene using published primers and QuikChange II Site-Directed Mutagenesis Kit. Forward- and reverse-antisense primers were then used to insert titin-specific sequences into the pAAV-U7smOpt vector with a free tail harboring canonical binding sites for hnRNP A1/A2 to increase exon-skipping efficiency (Supplementary Table 3) (37). Each cloned plasmid was confirmed by Sanger sequencing. 150 ng of each plasmid were transfected with X-tremeGENE 9 (Roche) in C2C12 myoblasts immediately after trypsinization (38). Day 10 myotubes were fixed in 2% PFA for 4 minutes then immunostained and imaged using the same conditions as with cryosectioned TA muscle; however, the antibody against the Z1Z2 region of titin was not used due to insufficient penetrance into myotubes.

Quantitative Real-time PCR (qRT-PCR)

Total RNA from iMS*Bmal1*$^{-/-}$ and iMS*Bmal1*$^{+/+}$ TA muscles was extracted using Trizol Reagent (Ambion) and purified using the RNeasy mini kit (Qiagen). 500 ng total RNA was reverse transcribed using SuperScript III first strand cDNA synthesis system (Invitrogen). Primers were generated using previously published sequences for *Rbm20* and *Rpl26* (20, 39). qRT-PCR was performed on a QuantiStudio 3 thermal cycler (Applied Biosystems) from 10 ng of cDNA in a total volume of 20 µL containing Fast SYBR Green Master Mix (Applied Biosystems) and 400 nM of each primer. *Rbm20* was normalized to corresponding *Rpl26*, and relative quantification was

calculated using the ΔΔCT method. Gene expression is shown as the relative fold change of expression in iMS*Bmal1*$^{-/-}$ muscle compared to iMS*Bmal1*$^{+/+}$ samples.

Western Blot

Protein lysates were prepared by homogenizing approximately 20 µg of TA muscle from iMS*Bmal1*$^{+/+}$ and iMS*Bmal1*$^{-/-}$ mice in RIPA buffer containing protease inhibitors using a Bullet Blender (Next Advance). 40 µg of total protein were loaded into each well for SDS-PAGE (10%). Proteins were transferred with a semidry apparatus (Bio-Rad) onto PVDF membrane then blotted overnight at 4˚C with anti-RBM20 antibody (Myomedix) or anti-γ-tubulin (Sigma) antibodies. Secondary antibodies were applied at room temperature for one hour and the blot was visualized using a ChemiDoc MP System (Bio-Rad). RBM20 bands were quantified with Image Lab software and normalized to the γ-tubulin loading control.

Targeted ChIP-PCR in Adult Skeletal Muscle from C57Bl/6J Mice

MYOD1, BMAL1, and CLOCK ChIP-seq data recently published by our lab were searched for binding peaks in *Rbm20* using UCSC Genome Browser (20–22). Following identification of overlapping peaks, putative regulatory regions identified by the ENCODE Registry of cis-Regulatory Elements were scanned for canonical E-box sequences 5'-CANNTG-3' (23). Primers flanking one of these E-box containing peaks in *Rbm20* were designed and used for ChIP-PCR to confirm binding.

For ChIP-PCR, approximately 800 mg of adult gastrocnemius muscle was homogenized in cell lysis buffer (10 mM HEPES, pH7.5, 10 mM MgCl2, 60 mM KCl, 300 mM sucrose, 0.1 mM EDTA, pH8.0, 0.1% Triton X-100, 1 mM DTT, protease inhibitors) and prepared as previously described (20). After pre-clearing with Protein A/G beads, supernatant was split into equal parts and incubated overnight at 4ºC with MYOD1 antibody, CLOCK antibody, BMAL1 antibody, or pre-immune serum prior to DNA recovery with a PCR purification kit (Qiagen). qRT-PCR was performed with *Rbm20* intron 1 primers. Data are presented as percent of input Ct, and significance was determined by comparing experimental ChIP values to those of the IgG control.

Generation of RBM20-AAV

Mouse *Rbm20* cDNA was cloned into pAAV-CMV with a C-terminal HA-tag and confirmed by Sanger sequencing. AAV was produced using transient transfection of HEK 293T cells and CsCl sedimentation by the University of Massachusetts Medical School Viral Vector Core as previously described (40). Vector preparations were determined by ddPCR, and purity was assessed by SDS-PAGE and silver staining (Invitrogen). Expression of RBM20-HA was confirmed in C2C12 myoblasts via western blot.

iMS*Bmal1*$^{fl/fl}$ mice were treated with tamoxifen or vehicle as described above. 4 weeks after treatment, mice were injected with AAV into the TA muscle. AAV was diluted in sterile PBS then 1 x 1012 GC of RBM20-AAV or 0.5 x 1012 GC of GFP-AAV were injected evenly throughout the entire TA of anesthetized mice. Muscles were collected 4 weeks after AAV injection and flash frozen in liquid nitrogen for protein analyses.

Statistics

All statistical analyses were performed using GraphPad Prism. Student's *t*-tests were used to compare two groups with *F*-tests to compare variance between groups. One-way ANOVA with Tukey's post-hoc analysis was used to detect significant differences in experiments with three groups. Figures were made using a combination of GraphPad Prism, ggplot2 and karyoploteR packages within R, and Adobe Illustrator. Values are reported as mean ± SEM. * $P < 0.05$, ** $P < 0.01$, *** $P < 0.005$.

Acknowledgments

We thank Dr. David Moraga and the University of Florida's Interdisciplinary Center for Biotechnology Research NextGen DNA Sequencing Core. We also thank Anisha Saripalli for help

with immunohistochemistry experiments and Dr. Christopher Wolff for commentary while preparing the original manuscript. This work was supported by National Institutes of Health grants F31AR070625 to LAR, R01AR066082 to KAE, DP5OD017865 to ETW, and the University of Florida. DWH and SL were supported by Leducq Foundation funding (13CVD04).

References

1. J. Bass, J. S. Takahashi, Circadian integration of metabolism and energetics. *Science (80-.).* (2010) https:/doi.org/10.1126/science.1195027.

2. M. Merrow, K. Spoelstra, T. Roenneberg, The circadian cycle: Daily rhythms from behaviour to genes. *EMBO Rep.* (2005) https:/doi.org/10.1038/sj.embor.7400541.

3. S. H. Yoo, *et al.*, PERIOD2::LUCIFERASE real-time reporting of circadian dynamics reveals persistent circadian oscillations in mouse peripheral tissues. *Proc. Natl. Acad. Sci. U. S. A.* (2004) https:/doi.org/10.1073/pnas.0308709101.

4. M. K. Bunger, *et al.*, Mop3 is an essential component of the master circadian pacemaker in mammals. *Cell* (2000) https:/doi.org/10.1016/S0092-8674(00)00205-1.

5. J. B. Hogenesch, Y. Z. Gu, S. Jain, C. A. Bradfield, The basic-helix-loop-helix-PAS orphan MOP3 forms transcriptionally active complexes with circadian and hypoxia factors. *Proc. Natl. Acad. Sci. U. S. A.* (1998) https:/doi.org/10.1073/pnas.95.10.5474.

6. K. Bozek, *et al.*, Regulation of clock-controlled genes in mammals. *PLoS One* (2009) https:/doi.org/10.1371/journal.pone.0004882.

7. B. H. Miller, *et al.*, Circadian and CLOCK-controlled regulation of the mouse transcriptome and cell proliferation. *Proc. Natl. Acad. Sci. U. S. A.* (2007) https:/doi.org/10.1073/pnas.0611724104.

8. H. Reinke, G. Asher, Crosstalk between metabolism and circadian clocks. *Nat. Rev. Mol. Cell Biol.* (2019) https:/doi.org/10.1038/s41580-018-0096-9.

9. J. J. McCarthy, *et al.*, Identification of the circadian transcriptome in adult mouse skeletal muscle. *Physiol. Genomics* (2007) https:/doi.org/10.1152/physiolgenomics.00066.2007.

10. J. L. Andrews, *et al.*, CLOCK and BMAL1 regulate MyoD and are necessary for maintenance of skeletal muscle phenotype and function. *Proc. Natl. Acad. Sci. U. S. A.* (2010) https:/doi.org/10.1073/pnas.1014523107.

11. E. A. Schroder, *et al.*, Intrinsic muscle clock is necessary for musculoskeletal health. *J. Physiol.* (2015) https:/doi.org/10.1113/JP271436.

12. B. A. Hodge, *et al.*, The endogenous molecular clock orchestrates the temporal separation of substrate metabolism in skeletal muscle. *Skelet. Muscle* (2015) https:/doi.org/10.1186/s13395-015-0039-5.

13. W. Guo, S. J. Bharmal, K. Esbona, M. L. Greaser, Titin diversity--alternative splicing gone wild. *J. Biomed. Biotechnol.* **2010**, 753675 (2010).

14. S. Schafer, *et al.*, Alternative Splicing Signatures in RNA-seq Data: Percent Spliced in (PSI). *Curr. Protoc. Hum. Genet.* (2015) https:/doi.org/10.1002/0471142905.hg1116s87.

15. W. Guo, *et al.*, RBM20, a gene for hereditary cardiomyopathy, regulates titin splicing. *Nat. Med.* (2012) https:/doi.org/10.1038/nm.2693.

16. H. Maatz, *et al.*, RNA-binding protein RBM20 represses splicing to orchestrate cardiac pre-mRNA processing. *J. Clin. Invest.* (2014) https:/doi.org/10.1172/JCI74523.

17. L. T. Denes, *et al.*, Culturing C2C12 myotubes on micromolded gelatin hydrogels accelerates myotube maturation. *Skelet. Muscle* (2019) https:/doi.org/10.1186/s13395-019-0203-4.

18. A. Bettadapur, *et al.*, Prolonged Culture of Aligned Skeletal Myotubes on Micromolded Gelatin Hydrogels. *Sci. Rep.* (2016) https:/doi.org/10.1038/srep28855.

19. S. Li, W. Guo, C. N. Dewey, M. L. Greaser, Rbm20 regulates titin alternative splicing as a splicing repressor. *Nucleic Acids Res.* (2013) https:/doi.org/10.1093/nar/gks1362.

20. B. A. Hodge, *et al.*, MYOD1 functions as a clock amplifier as well as a critical co-factor for downstream circadian gene expression in muscle. *Elife* (2019) https:/doi.org/10.7554/eLife.43017.

21. Y. Cao, *et al.*, Genome-wide MyoD Binding in Skeletal Muscle Cells: A Potential for Broad Cellular Reprogramming. *Dev. Cell* (2010) https:/doi.org/10.1016/j.devcel.2010.02.014.

22. B. M. Gabriel, *et al.*, Disrupted circadian core-clock oscillations in Type 2 Diabetes are linked to altered rhythmic mitochondrial metabolism. *bioRxiv*, 2021.02.24.432683 (2021).

23. F. Abascal, *et al.*, Expanded encyclopaedias of DNA elements in the human and mouse genomes. *Nature* (2020) https:/doi.org/10.1038/s41586-020-2493-4.

24. E. E. Terry, *et al.*, Transcriptional profiling reveals extraordinary diversity among skeletal muscle tissues. *Elife* (2018) https:/doi.org/10.7554/eLife.34613.

25. W. B. Isaacs, I. S. Kim, A. Struve, A. B. Fulton, Biosynthesis of titin in cultured skeletal muscle cells. *J. Cell Biol.* **109**, 2189–2195 (1989).

26. K. da Silva Lopes, A. Pietas, M. H. Radke, M. Gotthardt, Titin visualization in real time reveals an unexpected level of mobility within and between sarcomeres. *J. Cell Biol.* **193**, 785–798 (2011).

27. E. H. Lee, M. Gao, N. Pinotsis, M. Wilmanns, K. Schulten, Mechanical strength of the titin Z1Z2-telethonin complex. *Structure* **14**, 497–509 (2006).

28. C. C. Gregorio, *et al.*, “The NH 2 Terminus of Titin Spans the Z-Disc: Its Interaction with a Novel 19-kD Ligand (T-cap) Is Required for Sarcomeric Integrity” (1998).

29. P. S. Podobed, F. J. Alibhai, C.-W. Chow, T. A. Martino, Identification of Cardiac Clock-Controlled Genes Using Open Access Bioinformatics Data. *Circadian Regul. Myocard. Sarcomeric Titin-cap* **9**, 104907 (2014).

30. M. Wirianto, *et al.*, The GSK-3β-FBXL21 Axis Contributes to Circadian TCAP Degradation and Skeletal Muscle Function. *Cell Rep.* **32**, 108140 (2020).

31. J. J. McCarthy, R. Srikuea, T. J. Kirby, C. A. Peterson, K. A. Esser, Inducible Cre transgenic mouse strain for skeletal muscle-specific gene targeting. *Skelet. Muscle* (2012) https:/doi.org/10.1186/2044-5040-2-8.

32. C. M. Warren, P. R. Krzesinski, M. L. Greaser, Vertical agarose gel electrophoresis and electroblotting of high-molecular-weight protiens. *Electrophoresis* (2003) https:/doi.org/10.1002/elps.200305392.

33. D. Kim, B. Langmead, S. L. Salzberg, HISAT: A fast spliced aligner with low memory requirements. *Nat. Methods* (2015) https:/doi.org/10.1038/nmeth.3317.

34. M. I. Love, W. Huber, S. Anders, Moderated estimation of fold change and dispersion for RNA-seq data with DESeq2. *Genome Biol.* (2014) https:/doi.org/10.1186/s13059-014-0550-8.

35. C. Brun, *et al.*, U7 snRNAs induce correction of mutated dystrophin pre-mRNA by exon skipping. *Cell. Mol. Life Sci.* (2003) https:/doi.org/10.1007/s000180300047.

36. L. Echevarría, P. Aupy, A. Goyenvalle, Exon-skipping advances for Duchenne muscular dystrophy. *Hum. Mol. Genet.* (2018) https:/doi.org/10.1093/hmg/ddy171.

37. A. Goyenvalle, K. E. Davies, Engineering exon-skipping vectors expressing U7 snRNA constructs for Duchenne muscular dystrophy gene therapy. *Methods Mol. Biol.* (2011) https:/doi.org/10.1007/978-1-61737-982-6_11.

38. J. Escobedo, T. J. Koh, Improved transfection technique for adherent cells using a commercial lipid reagent. *Biotechniques* (2003) https:/doi.org/10.2144/03355bm06.

39. M. M. G. Van Den Hoogenhof, *et al.*, RBM20 mutations induce an arrhythmogenic dilated cardiomyopathy related to disturbed calcium handling. *Circulation* (2018) https:/doi.org/10.1161/CIRCULATIONAHA.117.031947.

40. M. Sena-Esteves, G. Gao, Introducing genes into mammalian cells: Viral vectors. *Cold Spring Harb. Protoc.* (2020) https:/doi.org/10.1101/pdb.top095513.

Figures and Tables

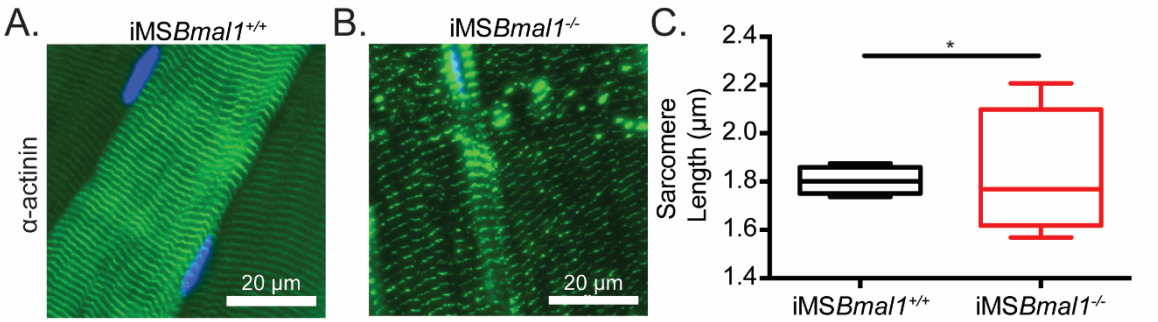

Figure 1. Sarcomere lengths are variable in iMSBmal1-/- muscle. Representative images from A. iMS*Bmal1*$^{+/+}$ and B. iMS*Bmal1*$^{-/-}$ tibialis anterior muscles. Muscles were longitudinally cryosectioned and stained with a primary antibody against α-actinin-2. C. Sarcomere lengths are significantly more variable as based on an F-test in iMS*Bmal1*$^{-/-}$ muscles compared to iMS*Bmal1*$^{+/+}$ controls. N = 4/group. * $P < 0.05$

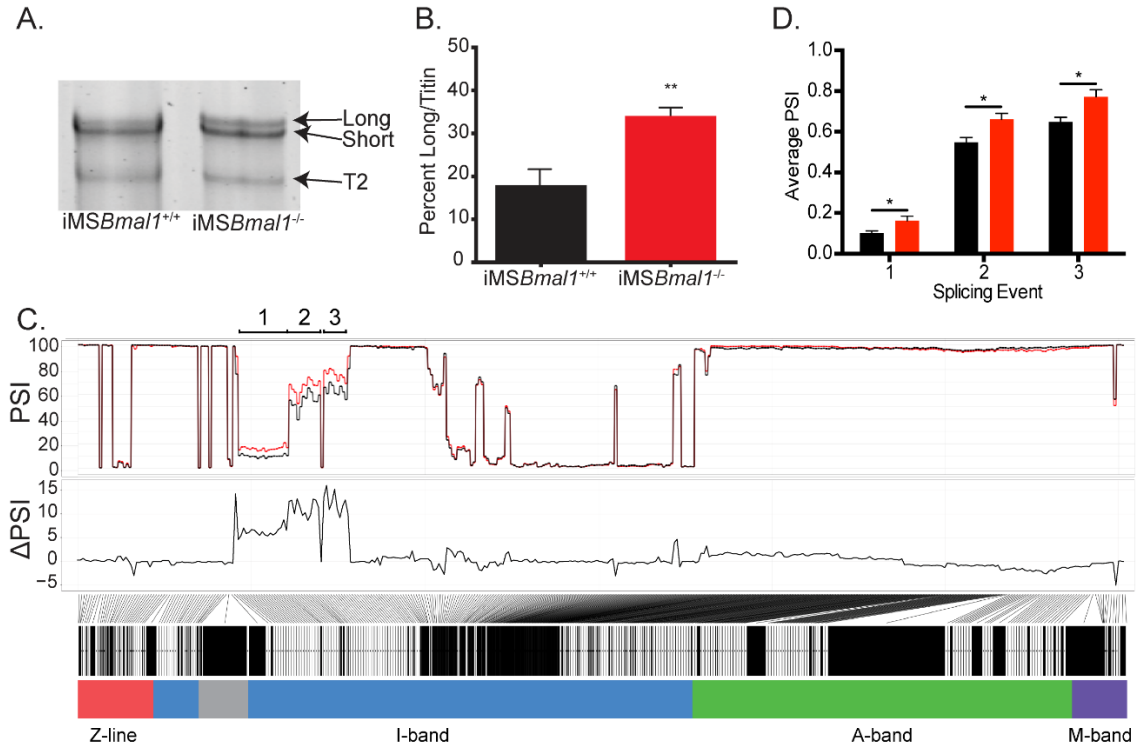

Figure 2. Skeletal muscle *Bmal1* knockout results in altered splicing of titin's spring region. A. SDS-VAGE was performed to measure titin protein isoform in iMS*Bmal1*$^{+/+}$ and iMS*Bmal1*$^{-/-}$ tibialis anterior muscles. B. Quantification of titin isoforms in these muscles shows a significant shift in titin isoform from a predominantly short isoform to a mix of long and short isoforms in iMS*Bmal1*$^{-/-}$ muscles but not iMS*Bmal1*$^{+/+}$ muscles (N = 8/group). C. Percent Spliced in (PSI) and ΔPSI of titin exons expressed in iMS*Bmal1*$^{+/+}$ and iMS*Bmal1*$^{-/-}$ skeletal muscle. Exons within the proximal Ig domain were included more often in iMS*Bmal1*$^{-/-}$ muscle compared to iMS*Bmal1*$^{+/+}$ muscle (N = 3/group). D. Average PSI across 3 splicing events in the proximal Ig domain of tibialis anterior muscle show increased exon inclusion in iMS*Bmal1*$^{-/-}$ mice compared to iMS*Bmal1*$^{+/+}$ controls. Each event is highlighted in Figure 2C. * $P < 0.05$ ** $P < 0.01$

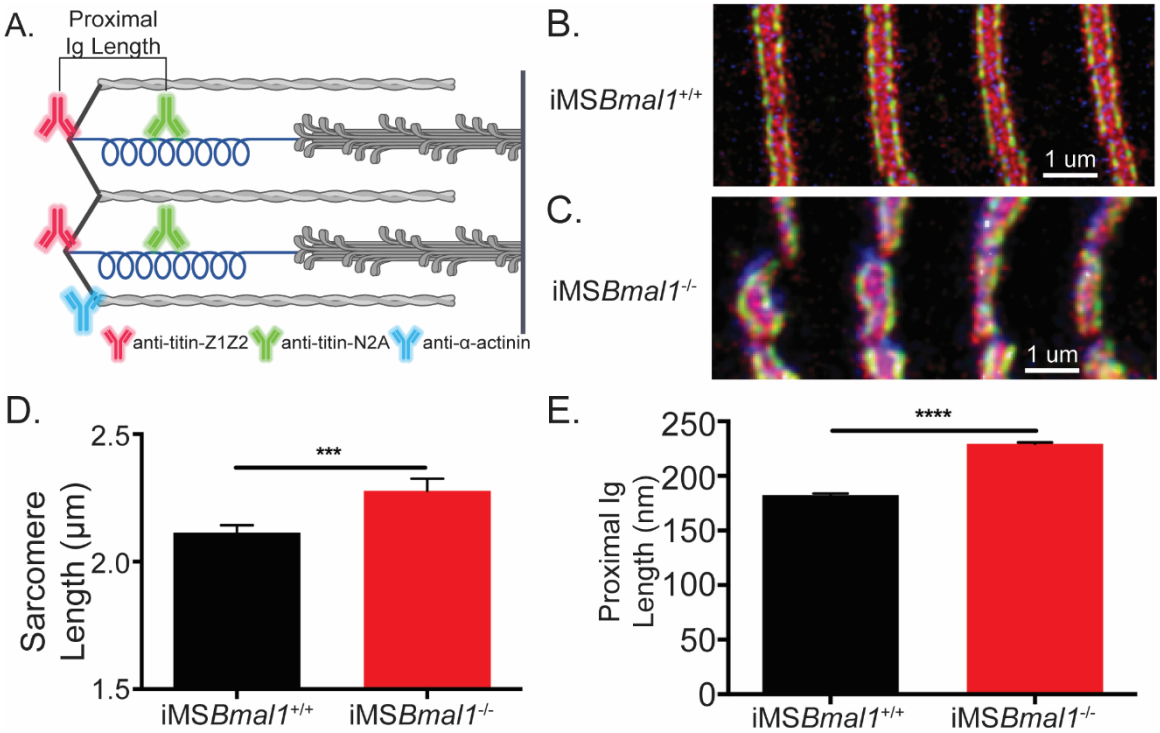

Figure 3. The change in titin's spring length in iMS*Bmal1*$^{-/-}$ muscle accounts for sarcomere length variability. A. Proximal Ig length was determined as the positional difference between the Z1Z2 domain of titin and the N2A domain of titin. These antibodies flank the proximal Ig domain. Created with BioRender.com Representative images of immunohistochemistry using titin-epitope specific and α-actinin-2 antibodies for B. iMS*Bmal1*$^{+/+}$ and C. iMS*Bmal1*$^{-/-}$ skeletal muscle. Green: N2A titin. Red: Z1Z2 titin. Blue: α-actinin-2. D. Sarcomere length variability is significantly lower in iMS*Bmal1*$^{+/+}$ compared to iMS*Bmal1*$^{-/-}$ skeletal muscle. E. A significantly longer proximal Ig length is correlated with this change in sarcomere length variability. N=250-350 sarcomeres/3 biological replicates per group. *** $P < 0.001$ **** $P < 0.0001$.

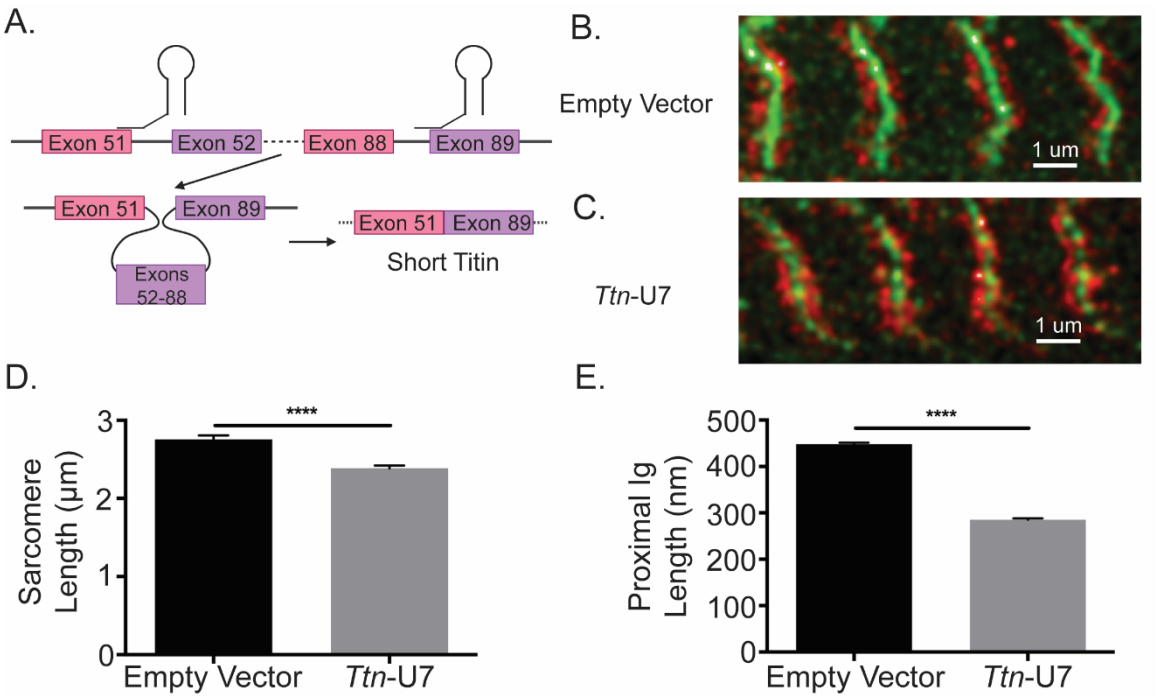

Figure 4. Directly shortening titin's proximal Ig domain length results in shorter sarcomeres in vitro. A. U7 snRNPs were designed to induce splicing or the proximal Ig domain with dysregulated splicing in iMS*Bmal1*$^{-/-}$ muscle. Created with BioRender.com Representative images of immunocytochemistry using a titin-epitope specific antibody and stably expressing eGFP-ACTN2 C2C12 myotubes that were transfected with an B. empty vector control or C. *Ttn*-U7 splicing factors. Green: α-actinin-2 Red: N2A titin. D. Sarcomere lengths were significantly shorter in myotubes transfected *Ttn*-U7 vectors compared to empty vector controls. E. *Ttn*-U7 vector transfection resulted in significantly shorter proximal Ig domain lengths in eGFP-ACTN2-C2C12 myotubes. **** $P < 0.0001$

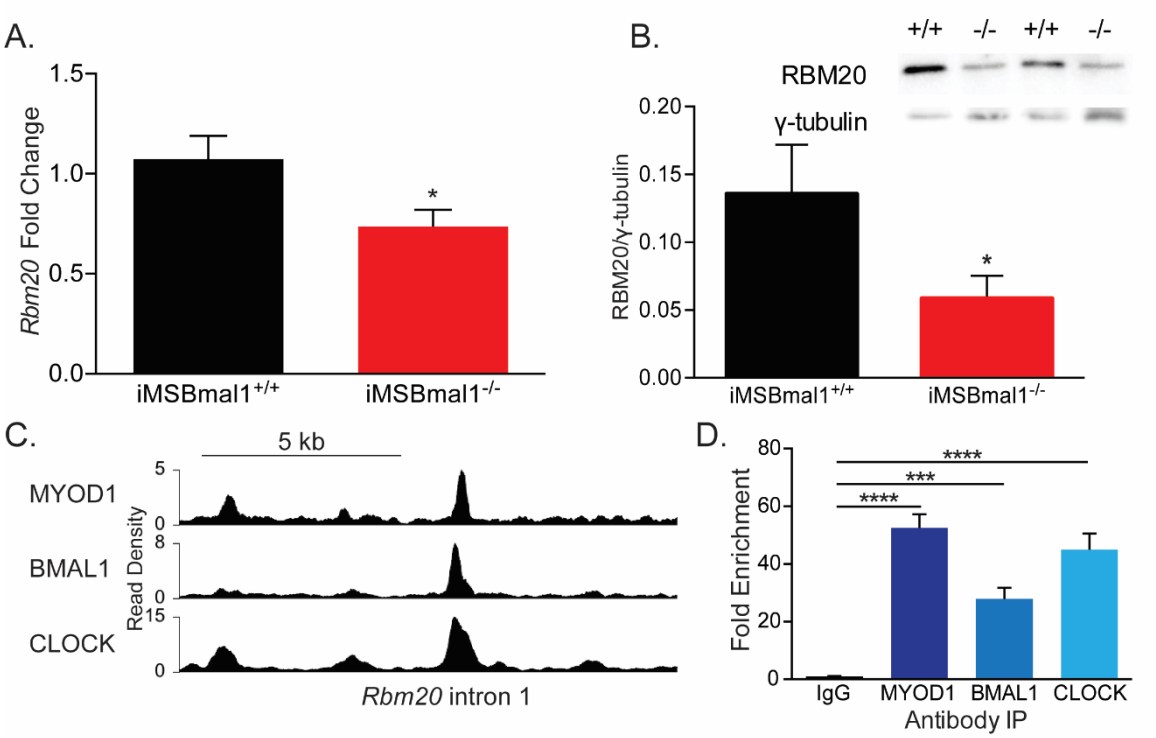

Figure 5. Rbm20 is targeted by the positive limb of the skeletal muscle molecular clock. A. *Rbm20* mRNA is decreased by 34% in iMS*Bmal1*$^{-/-}$ muscle compared to iMS*Bmal1*$^{+/+}$ muscle (N = 6-8/group). B. iMS*Bmal1*$^{-/-}$ muscle shows a 57% reduction in RBM20 protein levels compared to iMS*Bmal1*$^{+/+}$ control muscle (N = 4/group). C. Publicly available BMAL1, CLOCK, and MYOD1 ChIP-seq data were used to identify E-box elements in potential regulatory regions for *Rbm20*. A significant binding peak was found within intron 1 of this gene. D. ChIP-PCR confirms binding of each protein of the positive limb of the molecular clock at this site. * $P < 0.05$ ** $P < 0.01$ *** $P < 0.001$

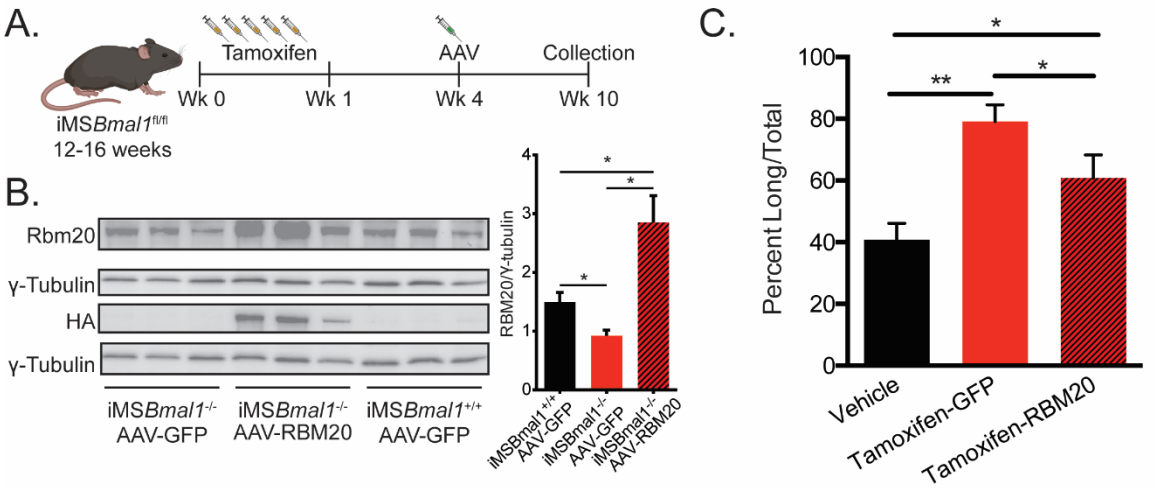

Figure 6. Rescuing RBM20 expression in iMS*Bmal1*$^{-/-}$ muscle restores titin spring length. A. Protocol for conditionally knocking out skeletal muscle Bmal1 and overexpressing RBM20. B. Transduction of AAV-RBM20 in iMS*Bmal1-/-* muscle increases RBM20 91% over iMS*Bmal1*$^{+/+}$ AAV-GFP muscle and 3-fold over iMS*Bmal1*$^{-/-}$ AAV-GFP muscle. C. Titin isoform expression is partially restored in iMS*Bmal1*$^{-/-}$ AAV-RBM20 muscle. * $P < 0.05$ ** $P < 0.01$